DISTINCT MECHANISMS OF LIPID BILAYER PERTURBATION INDUCED BY PEPTIDES DERIVED FROM THE MEMBRANE-PROXIMAL EXTERNAL REGION OF HIV-1 gp41.[†]

[†]This study was supported by Spanish MICINN (BIO2008-00772) and University of the Basque Country (GIU 06/42 and DIPE08/12).

Beatriz Apellániz[‡], *Shlomo Nir*[§], *and José L. Nieva*[‡*]

[‡]Unidad de Biofísica (CSIC-UPV/EHU) and Departamento de Bioquímica, Universidad del País Vasco, Aptdo. 644, 48080 Bilbao, Spain.

[§] Seagram Center for Soil and Water Sciences, Faculty of Agricultural, Food and Environmental Quality Sciences, The Hebrew University of Jerusalem, Rehovot 76100, Israel.

Running title: Pore-forming MPER peptides

*Corresponding author: José L. Nieva; Phone: +34 94 601 3353; Fax: +34 94 601 3360; E-mail: gbpniesj@lg.ehu.es

Abbreviations and textual footnotes:

[1]ANTS, 8-aminonaphtalene-1,3,6-trisulfonic acid sodium salt; DPX, p-xylenebis(pyridinium)bromide; Br_6-PSPC, 1-palmitoyl-2-stearoyl(6,7)dibromo-sn-glycero-3-phosphocholine; Br_{11}-PSPC, 1-palmitoyl-2-stearoyl(11,12)dibromo-sn-glycero-3-phosphocholine; CD, circular dichroism; DPC, Dodecylphosphocholine; FP, fusion peptide; HIV-1 human immunodeficiency virus type-1; LUV, large unilamellar vesicles; MPER, membrane-proximal external region; POPC, 1-palmitoyl-2-oleoylphosphatidylcholine; PreTM, pretransmembrane; SPM, sphingomyelin; TMD, transmembrane domain.

Abstract

The conserved, membrane-proximal external region (MPER) of the human immunodeficiency virus type-1 envelope glycoprotein 41 subunit is required for fusogenic activity. It has been proposed that MPER functions by disrupting the virion membrane. Supporting its critical role in viral entry as a membrane-bound entity, MPER constitutes the target for broadly neutralizing antibodies that have evolved mechanisms to recognize membrane-inserted epitopes. We have analyzed here the molecular mechanisms of membrane permeabilization induced by N-preTM and PreTM-C, two peptides derived from MPER sequences showing tendency to associate with the bilayer interface or to transfer into the hydrocarbon-core, respectively. Both peptides contained the full epitope sequence recognized by the 4E10 monoclonal antibody (MAb4E10), which was subsequently used to probe peptide accessibility from the water phase. Capacities of N-preTM and PreTM-C for associating with vesicles and inducing their permeabilization were comparable. However, MAb4E10 specifically blocked the permeabilization induced by N-preTM, but did not appreciably affect that induced by PreTM-C. Supporting the existence of different membrane-bound lytic structures, N-preTM was running as a monomer on SDS-PAGE and induced graded release of vesicular contents, whereas PreTM-C migrated on SDS-PAGE as dimers and permeabilized vesicles following an all-or-none mechanism, reminiscent of that underlying melittin-induced membrane lysis. These results support the functional segmentation of gp41 membrane regions into hydrophobic subdomains, which might expose neutralizing epitopes and induce membrane-disrupting effects following distinct patterns during the fusion cascade.

The envelope glycoprotein (Env) mediates merging of viral and cellular membranes at the beginning of the human immunodeficiency virus type-1 (HIV-1)[1] infectious cycle. The most widely accepted fusion mechanism postulates that the formation of trimeric helical hairpins by the ectodomains of several gp41 transmembrane subunits might bring cell and viral membranes to close apposition (reviewed in (*1-3*)). It is also assumed that the activation of the fusion cascade exposes to the medium the amino-terminal hydrophobic gp41 region or fusion peptide (FP, (*4*)), which subsequently inserts into the cell target membrane. FP insertion into the target cell membrane is thought to perturb its bilayer organization making it more prone for merging and fusion-pore opening (reviewed in (*5-7*)).

Mutagenesis studies revealed the existence of an additional hydrophobic and conserved region in gp41 ectodomain that was also functional in fusion (*8-11*). This region, termed as MPER or PreTM, is located preceding the transmembrane domain (TMD) (*8, 12*). The high content in aromatic amino acids led to the prediction that the MPER sequence could favorably interact with the external monolayer of the virion membrane (*12, 13*). This possibility was supported by nuclear magnetic resonance studies of MPER-derived peptides (*14, 15*) and cryoelectron tomography analyses of the native envelope spikes (*16*). Biophysical characterization of representative peptides further suggested that MPER insertion may perturb the lipid bilayer organization (*12, 13, 17*). Studies by our group demonstrated that the MPER-representing HIV_c peptide could induce permeabilization of large unilamellar vesicles (LUV) in the range of 1:10000 peptide-to-lipid ratios, i.e., with membrane doses that are relevant for the low spike density existing in the virion envelope (*18*). This phenomenon was stimulated by the presence of sphingomyelin (SPM), a phospholipid present at high quantities in the

virion envelope (*19*). It was therefore proposed that MPER-activity might contribute to the membrane-restructuring required for fusion-pore formation (recently reviewed in (*20*)).

The functional importance of MPER lytic activity for gp41-induced fusion has been recently demonstrated by Vishwanathan and Hunter (*10*). These authors designed gp41 chimeras that replaced all or part of MPER with indolicidin-based sequences. Indolicidin is a Trp-rich, antimicrobial and hemolytic peptide that forms pores in membranes (reviewed in (*21*)). Thus, indolicidin and MPER have in common the unusual high number of tryptophans and their capacity to permeabilize membranes. These authors hypothesized that if MPER-induced membrane perturbations were required for gp41 fusogenic function, its replacement with indolicidin would produce functional Env glycoprotein. Some of the produced gp41 chimeras indeed retained fusion activity, therefore demonstrating that MPER can be replaced by a membrane-disruptive foreign sequence and preserve its biological function (*10*).

The recent observation that HIV-1 neutralizing MAb-s 2F5 and 4E10 block peptide-induced liposome permeabilization by associating physically with vesicles adds further support to the idea that MPER membrane perturbing properties are key to gp41 fusion function (*22, 23*). These antibodies recognize lineal epitope sequences within MPER (reviewed in (*24*)). Nonetheless, both antibodies have evolved mechanisms for shallow insertion into the membrane interface, which allow them to bind epitope sequences inserted therein (*15, 23, 25*).

Here we present results consistent with different mechanisms of membrane interaction and perturbation by 4E10 epitope-containing MPER sequences elongated at their N- or C-terminus (Figure 1). The representative N-preTM and PreTM-C peptides showed comparable partitioning, depth of Trp insertion and permeabilizing capacity in

1-palmitoyl-2-oleoylphosphatidylcholine (POPC) vesicles. However, MAb4E10 specifically blocked the membranolytic activity of N-preTM, but did not affect that displayed by PreTM-C, therefore suggesting that 4E10 epitope gets occluded within the lytic structures assembled in membranes by the latter peptide. The existence of two distinct membrane-bound lytic structures was supported by the fact that the pore-forming mechanisms followed by the two peptides were different. N-preTM induced graded release of vesicular contents, consistent with the induction of local and transient membrane lesions. In contrast, PreTM-C showed a tendency to self-associate and induced leakage of aqueous contents following an all-or-none mechanism. The latter peptide emulated the mechanism and size of the permeating pores generated by the cytolytic melittin in POPC:SPM vesicles, but was comparatively less efficient, as evidenced by the lower membrane-surface aggregation constants (K_s) that were deduced by the mathematical modeling of the leakage process. We conclude that the particular MPER hydrophobicity distribution might sustain distinct membrane-disrupting activities along the gp41-induced fusion cascade.

Materials and Methods

Materials

The MPER-derived N-preTM and PreTM-C peptides displayed in Figure 1 and the derived mutant sequences, NEQELLELDKWASLWNAANITNWLWYIK (N-preTM$_{mut}$) and KKKNAADITNWLWYIKLFIMIVGGLVKK (PreTM-C$_{mut}$), were produced by solid-phase synthesis using Fmoc chemistry as C-terminal carboxamides and purified by HPLC. Melittin was purchased from NeoMPS (Strasbourg, France). 1-palmitoyl-2-oleoylphosphatidylcholine (POPC), sphingomyelin (SPM), 1-palmitoyl-2-stearoyl(6,7)dibromo-sn-glycero-3-phosphocholine (Br$_6$-PSPC) and 1-palmitoyl-2-stearoyl(11,12)dibromo-sn-glycero-3-phosphocholine (Br$_{11}$-PSPC) were purchased from Avanti Polar Lipids (Birmingham, AL, USA) while Dodecylphosphocholine (DPC) was from Anatrace (Maumee, OH, USA). The 8-aminonaphtalene-1,3,6-trisulfonic acid sodium salt (ANTS) and p-xylenebis(pyridinium)bromide (DPX) were obtained from Molecular Probes (Junction City, OR, USA). MAb4E10 was obtained from Polynum Inc., (Vienna, Austria). All other reagents were of analytical grade.

Circular Dichroism

Circular dichroism (CD) measurements were obtained from a thermally-controlled Jasco J-810 circular dichroism spectropolarimeter calibrated routinely with (1S)-(+)-10-camphorsulfonic acid, ammonium salt. Stock peptide samples in DMSO were lyophilized and subsequently dissolved at a final concentration of 0.03 mM in 2 mM Hepes (pH, 7.4) buffer containing 20 mM DPC. Spectra were measured in a 1 mm path-

length quartz cell initially equilibrated at 25 ºC. Data were taken with a 1 nm band-width at 100 nm/min speed, and the results of 20 scans were averaged.

Lipid vesicle assays

Large unilamellar vesicles (LUV) were prepared according to the extrusion method in 5 mM Hepes, 100 mM NaCl (pH 7.4) using membranes with a nominal pore-size of 0.1 µm. Distribution of sizes, estimated by quasielastic light scattering using a Malvern Zeta-Sizer Nano ZS instrument (Malvern Instruments, Malvern, UK), revealed mean diameters of 97 and 99 nm for POPC and POPC: SPM (1:1 mol:mol) vesicles, respectively. The vesicle size distribution did not significantly change upon the addition of peptides at the highest tested doses (i.e., 1:100 peptide-to-lipid ratio).

Peptide incorporation into membranes under our experimental conditions was evaluated by monitoring the change in the emitted Trp-fluorescence. Corrected spectra were recorded using a FluoroMax-3 (Jobin Ybon, Horiba) with excitation set at 280 nm and 2-nm slits. Partitioning curves were subsequently computed from the fractional changes in emitted Trp-fluorescence when titrated with increasing lipid concentrations. The apparent mole fraction partition coefficients, $K_{x(app)}$, were determined by fitting the experimental values to a hyperbolic function (*26*):

$$F/F_0 = 1 + \frac{[(F_{max}/F_0)-1]\,[L]}{K + [L]} \qquad [1]$$

where [L] is the lipid concentration and K is the lipid concentration at which the bound peptide fraction is 0.5. Therefore, $K_{x(app)} = [W]/K$ where [W] is the molar concentration of water.

Penetration level of the peptide into the bilayer core was inferred from the Trp fluorescence quenching by the hydrophobic matrix-residing brominated phospholipids (*27*). These experiments were carried out using vesicles containing increasing POPC fractions substituted for the brominated phospholipids Br_6-PSPC or Br_{11}-PSPC, as described by De Kroon et al. (*28*). Data obtained for each brominated lipid were analyzed according to the Stern-Volmer equation for collisional quenching:

$$F_0/F = 1+K_{sv}[Q] \qquad [2]$$

Where F_0 and F are the fluorescence intensities in the absence and presence of quencher, [Q] is the molar concentration of quencher, and K_{sv} is the Stern-Volmer quenching constant.

Vesicle permeabilization was assayed by monitoring the release to the medium of encapsulated fluorescent ANTS (ANTS/DPX assay (*29*)). LUV containing 12.5 mM ANTS, 45 mM DPX, 20 mM NaCl and 5 mM Hepes were obtained by separating the unencapsulated material by gel-filtration in a Sephadex G-75 column that was eluted with 5 mM Hepes and 100 mM NaCl (pH 7.4). Fluorescence measurements were performed by setting the ANTS emission at 520 nm and the excitation at 355 nm. A cutoff filter (470 nm) was placed between the sample and the emission monochromator. The baseline leakage (0%) corresponded to the fluorescence of the vesicles at time 0, while 100% leakage was the fluorescence value obtained after addition of Triton X-100 (0.5% v/v).

For pore-size determination, FITC-dextran probes with different sizes were encapsulated in vesicles at self-quenching concentrations as described by Basanez et al. (*30*).

Determination of leakage mechanism

The ANTS/DPX requenching assay was used to determine the mechanism of leakage as previously described (*31-34*). The goal of this assay is to establish the dependence of the quenching inside vesicles (Q_{in}) on the ANTS fraction outside vesicles (f_{out}). Q_{in} is defined as the ratio between the ANTS fluorescence inside vesicles at any time (F_i) and its maximum possible value in the absence of DPX (F_i^{max}). Q_{in} remains constant and low for any f_{out} value when peptide-induced leakage follows an "all-or-none" mechanism, i.e., the population of vesicles consists of those that did not leak at all, and those releasing all of their aqueous contents. An increase of Q_{in} as a function of f_{out} reveals a dilution of both quencher and probe in the lumen of the vesicles, indicating that the leakage mechanism is "graded", in which vesicles lose some of their contents. In brief, peptides were assayed within a range of concentrations allowing final leakage extents below 100 % (see Figures 2D and 6B). The peptides were added to stirring mixtures containing 100 μM lipid vesicles with entrapped ANTS (5 mM) and DPX (8 mM) in 5 mM Hepes. Peptides and vesicles were incubated until the fluorescence signal leveled off (typically for 60 minutes). Then, the decrease in ANTS fluorescence intensity was recorded in each sample upon sequential quenching of ANTS outside vesicles by externally added DPX (25 μl aliquots from a 45 mM stock solution were added 4 times). Subsequently, an excess Triton X-100 (25 μl from a 10% w/v stock) was added to establish the fluorescence intensity corresponding to complete leakage. Fluorescence intensities were finally corrected for dilution. The methodology followed to determine Q_{in} and f_{out} parameters from these ANTS fluorescence values has been detailed by Ladokhin et al. (*33*).

Analysis of leakage via pore formation

PreTM-C-induced leakage extents were analyzed according to a mathematical model of pore formation as previously described (*35, 36*). In brief, the model assumes that the peptides added into a vesicle suspension bind, become incorporated within the bilayer, and aggregate. When an aggregate within a membrane has reached a critical size, i.e., it consists of M peptides, a pore can be created within the membrane, and leakage of encapsulated molecules can occur. It is assumed that the process of peptide binding is rapid and once a pore has been formed in a vesicle, all its contents will leak quickly. Thus, this leakage must be characterized by an "all-or-none" mechanism. Furthermore, the leakage must terminate after a certain period to yield final extents, which depend on peptide-to-lipid ratios. The rate and extent of leakage are assumed to be limited by the rate and extent of formation of surface aggregates of M or more peptides. The number M and geometrical considerations dictate the upper size of leaking molecules. In most of the cases the surface aggregation of the peptides is not irreversible and depends on $K_s = C/D$, in which C and D denote on and off rate constants of surface aggregation.

In a previous study we demonstrated that this model applied particularly well to melittin-induced leakage of PC:SPM vesicles (*37*). The calculations, which employ the parameters M (pore size) and K_s (degree of surface reversibility) use as an input the partitioning of the peptide and size distribution of vesicles. The calculations simulate the final extents of leakage as a function of lipid-to-peptide ratios.

ELISA

For the enzyme-linked immunosorbent assay (ELISA), peptides were dissolved in phosphate-buffered saline (PBS) and immobilized (100 µl/well) overnight in C96 Maxisorp microplate wells (Nunc, Denmark) at a concentration of 1.4 µM. Prior to incubation with the MAb4E10, the plates were blocked for 2 h with 3 % (w/v) bovine-serum albumin in PBS. The binding of the MAb was detected with an alkaline phosphatase-conjugated goat anti-human immunoglobulin (Pierce, Rockford, IL, USA), which then catalyzed a color reaction with the p-nitrophenyl phosphate substrate (Sigma, St. Louis, MO, USA) that could be measured by absorbance at a wavelength of 405 nm in a Synergy HT microplate reader (Bio-TEK Instruments Inc., VT, USA).

Results:

Hydrophobicity distribution within gp41pre- and transmembrane regions and design of the MPER peptides

Figure 1 displays the hydrophobicity distribution along gp41 MPER-TMD regions. The use of the Wimley-White (WW) hydrophobicity scale with a sliding window of 5 amino acids (black line) in combination with the moment calculated for a 3-turn α-helix (red-dotted line) reveals the existence of an amino-teminal amphipathic-at-interface helix (red cylinder), followed by a fully hydrophobic-at-interface stretch (green cylinder). The plot also displays the mean hydrophobicity calculated with the same sliding window of 5 amino acids and the Kyte-Doolittle (KD) scale (blue line). KD hydrophobicity distributes into two peaks that span the TMD region (blue cylinders). The first peak roughly spans the core region, which is more conserved than the rest of the TMD and buried into the lipid bilayer according to previously proposed models (*38*). Thus, it is inferred that MPER-derived sequences combining either the red and green subdomains or the green subdomain with the following blue TMD stretch would adopt different bilayer topologies. This prediction is supported by the free energy values computed for these sequences (Table 1). The free energy change of transferring from interface to octanol calculated for the 656-683 sequence is positive, suggesting that the process of transferring this gp41 region from the interface into the hydrocarbon-core would be unfavorable (*39*). In contrast, the same energy value calculated for the

671-693 sequence is negative, which would be consistent with its tendency for inserting into the bilayer matrix (*39*).

The effect of these bilayer-location tendencies on MPER-membrane interaction and pore-forming activity was experimentally analyzed using N-preTM and PreTM-C peptides (sequences displayed in Figure 1, bottom). To increase water-solubility, PreTM-C incorporated 5 additional Lys residues, and Asn674 substituted by Asp, a residue that is present in this position in several viral strains. Furthermore, both peptides contained the full-length 4E10 epitope, which allowed comparatively assessing MAb accessibility to membrane-bound sequences as previously described (*22, 23*). The analysis of pore-formation mechanism requires the use of dispersed vesicle populations (i.e., it has to be performed in the absence of peptide-induced aggregation or fusion, see for a discussion reference (*31*)). POPC and POPC:SPM (1:1 mol:mol) LUV were therefore selected as suitable targets for our studies, since these vesicles had been previously shown not to be aggregated or fused by MPER-derived peptides (*18*). Accordingly, none of the peptides altered the size-distribution of these vesicles at the highest assayed doses (not shown). In addition, it was inferred that the effect of the additional cationic residues would be minimal on the interactions of PreTM-C with the electrically neutral vesicles composed of zwitterionic lipids.

Association with vesicles and lytic activity of MPER-derived N-preTM and PreTM-C peptides

Titration experiments were first performed to compare N-preTM and PreTM-C association with membranes (Figures 2A and B). Membrane association was evidenced

by the changes in the fluorescence Trp spectrum obtained in the presence of POPC LUV (Figure 2A). For both peptides the fluorescence intensity increased and its maximum shifted towards lower wavelengths in the presence of vesicles. The corresponding partitioning curves disclosed $K_{x(app)}$ values higher than 10^6 for both peptides (Figure 2B). Thus, both MPER-derived peptides incorporated to similar extents into POPC vesicles under our experimental conditions.

Application of brominated lipid at two different positions along the acyl chains provided further information on the membrane topology of N-preTM and PreTM-C (Figure 2C). These experiments were performed at a 1:100 peptide-to-lipid ratio, i.e., under conditions allowing the efficient incorporation of both peptides into vesicles (ca. 94 and 92 % of the added N-preTM and PreTM-C, respectively). The Stern-Volmer representations of the fluorescence quenching displayed in Figure 2C revealed higher quenching constants for the Br_6-PSPC lipid in both cases. In POPC bilayers, the distance of the bromines from the head-group-hydrocarbon core boundary are 3.5 and 8.0 Å for 6,7- and 11,12-BRPC, respectively (*40*). Thus, these results would be consistent with the predicted tendency of Trp residues for locating close to the membrane-interface/hydrocarbon-core boundary (*39*). In addition, K_{sv} values were overall lower for N-preTM, which suggests a lower accessibility of this peptide's N-terminal Trp residues to the quenchers.

Finally, leakage experiments demonstrated the comparable membrane-permeabilizing capacities of both peptides (Figure 2D). N-preTM and PreTM-C induced 50 % ANTS leakage from POPC LUVs at peptide-to-lipid mole ratios of ca. 1:200 and 1:300, respectively. Thus, even though PreTM-C showed a somewhat higher potency than N-preTM, overall both peptides could be considered to induce effective LUV

permeabilization within the same range of peptide-to-lipid ratios (i.e., from 1:1,000 to 1:100).

Accessibility to MAb4E10 from the water phase.

The previous results indicate comparable capacities of N-preTM and PreTM-C for associating with, inserting into and permeabilizing the membrane. The accessibility of the membrane-bound sequences to MAb4E10 was next assessed based on the antibody's capacity to block ongoing leakage promoted by epitope-containing peptides (*22, 23*). In order to demonstrate the involvement of specific epitope recognition in the blocking process, the analysis included sequences in which Ala substituted for N-preTM Trp17 and Phe18 (N-preTM$_{mut}$), or PreTM-C Trp5 and Phe6 (PreTM-C$_{mut}$). These residues are crucial for the neutralizing activity of the MAb4E10 (*41*). ELISA studies confirmed the failure of the MAb4E10 to recognize N-preTM$_{mut}$ and PreTM-C$_{mut}$ while it efficiently bound to plates coated with the wild-type variants (Figure 3A). ELISA results also confirmed comparable binding of MAb4E10 to N-preTM (untagged) and PreTM-C (tagged), thereby suggesting that epitope recognition was unaffected by the presence of the added Lys residues or the Asn x Asp mutation.

The capacity of MAb4E10 to block vesicle permeabilization induced by these variants was then evaluated in POPC LUV (Figure 3B). In accordance with the specific recognition in membranes, the MAb4E10 blocked ongoing leakage induced by N-preTM, but not that induced by the mutant variant N-preTM$_{mut}$. Conversely, the antibody exerted almost no effect on the leakage processes induced by PreTM-C or PreTM-C$_{mut}$. In order to rule out the incapacity of MAb4E10 for binding PreTM-C

under the leakage assay conditions, the blocking protocol was varied (Figure 3C). Pre-incubation in solution of peptides with MAb4E10 prior to LUV addition, inhibited leakage induced by both wild-type sequences, N-preTM and PreTM-C (top panels). Supporting that specific epitope-recognition was also sustaining this inhibitory effect, pre-incubation in solution with the antibody did not appreciably affect the leakage induced by the mutant variants (bottom panels). In conclusion, even though the Trp-rich 4E10 epitope sequence present in both peptides was predicted to insert to a similar depth into the lipid bilayer (Figure 2), it lost accessibility to the MAb only upon PreTM-C association with membranes (Figure 3). One possible explanation for this PreTM-C specific effect might be the formation by this peptide of a distinct membrane-bound lytic structure inaccessible to MAb4E10. The results presented below would sustain such an option.

Secondary structure and peptide oligomerization

The circular dichroism results displayed in Figure 4 confirmed that both peptides adopted main helical conformations in contact with the membrane-mimicking DPC micelles. However, the higher absorption at 192 and 222 nm together with an increase in the $[\theta]_{222}/[\theta]_{208}$ ellipticity ratio might indicate a somewhat higher helicity and/or peptide self-association in the case of PreTM-C (*42, 43*). Alternatively, the existence of minimum located at ca. 219 nm is compatible with a contribution of extended chains to this peptide's spectrum.

Supporting different organizations in the low-polarity environment provided by SDS micelles, PreTM-C migrated as dimers (≈ 7 kDa) on Tris-tricine SDS-PAGE (Figure 5). The electrophoretic mobility of this peptide was actually comparable to that

of melittin used as a control, which also displayed a band consistent with that of approximately a dimer (≈ 6 kDa). In contrast, under these experimental conditions the N-preTM sample displayed a band corresponding to a monomer (≈ 3.6 kD). Putative differences in mobility due to the particular amino acid composition of each peptide rather to their size could be dismissed given the fact that PreTM-C monomers (≈ 3.5 kD) could also be observed when loaded on gels at low peptide concentrations (lane 1).

Mechanism of membrane permeabilization by N-preTM and PreTM-C peptides

Inclusion of SPM in the lipid composition was previously demonstrated to stimulate vesicle leakage induced by melittin and the MPER-derived HIV_c peptide (*18, 37*). Figure 6 compares the lytic activities of N-preTM and PreTM-C peptides measured in POPC:SPM (1:1) LUV. Titration experiments demonstrated that N-preTM and PreTM-C incorporated into POPC:SPM vesicles to similar extents, and that inclusion of SPM in the bilayer composition did not importantly affect the partitioning process (Figure 6A). At the added 1:500 peptide-to-lipid mole ratio both peptides induced leakage more readily in POPC:SPM vesicles than in pure POPC (top panels in Figure 6B). Inclusion of SPM in the vesicle composition reduced the peptide-to-lipid ratio required to induce 50% ANTS release to values below 1:1,000 in both cases (Figure 6B, bottom panels). Thus the peptide dose required to permeabilize POPC:SPM LUVs was about one order of magnitude lower than that required to permeabilize POPC LUV (Figure 2D). Moreover, both peptides induced POPC:SPM LUV leakage above the background level at 1:10,000 peptide-to-lipid ratio, and therefore, could be considered to be active at membrane doses relevant for the low spike density existing in the virion membrane (*44*).

The mechanism of pore formation in vesicles was next analyzed using the requenching method (*31-33*) (Figure 7). This method allowed discerning between "all-or-none" and "graded" mechanisms of leakage. Leakage according to an "all-or-none" mechanism denotes the assembly of peptides into pore structures capable of permeabilizing the bilayer continuously. In this case, some vesicles in the population release all their aqueous contents, while the rest conserve the permeability barrier intact. On the other hand, the existence of a "graded" mechanism reflects a transient perturbation of the permeability barrier coupled to the insertion and/or structuring of peptides within the bilayer, i.e., the membrane-bound peptide is not lytic when the system reaches equilibrium. This interaction induces only partial release of aqueous contents and, therefore, dilution of the encapsulated probes within the lumen of the vesicles.

The data displayed in Figure 7 demonstrate that N-preTM and PreTM-C permeabilized vesicles following different mechanisms, and that these mechanisms were the same for POPC and POPC:SPM vesicles. The Q_{in} parameter remained unchanged at all f_{out} values in the case of PreTM-C-induced leakage of POPC and POPC:SPM vesicles (empty circles and horizontal dashed lines in both panels). This pattern was reproduced by melittin (squares and horizontal dashed lines), a peptide that was previously shown by others to induce "all-or-none" leakage in POPC vesicles (*45-47*). Thus our data are consistent with analogous "all-or-none" mechanisms operating in the processes of leakage induced by PreTM-C and melittin in both types of vesicles. In sharp contrast, Q_{in} increased with f_{out} in the case N-preTM interacting with POPC or POPC:SPM vesicles (filled circles and continuous lines), which implies the existence of a graded release of contents in this case (*33, 34*). As shown in the plots (continuous

lines), the experimental values obtained for both types of vesicles could be fitted to a graded leakage model with the preference for DPX release ($\alpha > 1$, see reference (*33*)).

The finding that PreTM-C-induced leakage obeyed an all-or-none mechanism substantiated for this particular case the quantitative analysis of the process according to the mathematical pore-model developed by Nir (*35, 36, 48*) (Table 2 and Figure 8). For PreTM-C-induced leakage of POPC and POPC:SM (1:1) vesicles, final extents of leakage as a function of the peptide dose could be optimally fitted to hexameric (M=6) and octameric (M=8) pore models. Higher surface aggregation constant (K_s) values were obtained for POPC:SPM vesicles, indicating a lower degree of reversibility of PreTM-C surface aggregation than in the POPC system. This observation would be consistent with a larger membrane-bound peptide population participating in the assembly of lytic pores in the former case. The highest pore-forming efficiency for the bound PreTM-C peptide was observed for M=8 in POPC:SPM vesicles. Under these conditions, the estimated K_s value (ca. 0.04) denotes higher levels of reversibility of surface aggregation than melittin or GALA peptides (*35, 37, 48*), but lower than those reported for pardaxin (*49*).

Thus, the quantitative analysis above suggests that PreTM-C-induced LUV permeabilization might involve pores with a preferential size (6-8 monomers). Accordingly, the results displayed in Figure 9 support the concept that vesicles treated with this peptide pose a limit on the size of molecules able to leak out (top panel). This size-limit was determined by assaying the leakage from POPC:SPM LUV encapsulating solutes with different MW (*30, 34*). PreTM-C-induced leakage of FITC-dextran probes was severely restricted and decreased with the size of the encapsulated solute. For instance, most of the FD-40 probe (80-90%) was retained in the vesicles at doses inducing total release of ANTS. According to the pore model (*35, 36, 48*) if M is the

minimal number of peptides required for the leakage of molecules of a certain size, then there might be a certain though smaller probability for the leakage of larger molecules, since pores consisting of a larger number of peptides can exist. This would explain the observed partial release of the bigger solutes. The selection on the size of the leaking molecules also depends on the geometrical structure of the peptide. Notably, N-preTM-induced leakage was overall less restricted by the size of the encapsulated solutes (bottom panel), which emphasizes the different mechanism underlying the process.

Discussion

The gp41 MPER domain is targeted by antibodies that display broadly neutralizing activity and plays a critical role in HIV-1 fusion by perturbing the architecture of the bilayer envelope (recently reviewed in (*20, 24*)). The results in the present work are consistent with the idea that the tendency to remain associated with the membrane-interface, or to transfer into the bilayer hydrocarbon core (Table 1), might modulate MPER epitope accessibility and its bilayer-perturbing activity. In the membrane-bound state, the 4E10 epitope-spanning, Trp-rich strip adopts similar bilayer topologies within the representative N-preTM and PreTM-C peptides (Figure 2A-C). In addition, these two peptides displayed comparable capacities for disrupting the membrane (Figure 2C), an observation that would be in accordance with the proposed MPER role during fusion (*10, 20*) and the implication of the N-terminal TMD sequence in this process (*38, 50*). However, upon association with membranes, the N-preTM sequence could be specifically blocked by the 4E10 antibody, as evidenced from the inhibition of ongoing leakage induced by this peptide, while the 4E10 epitope appeared not to be accessible within the lytic structures assembled by PreTM-C in the bilayer (Figure 3).

Analysis of the mechanism of pore formation by the requenching assay (*31-34*) proved that N-preTM induces partial release of the vesicular aqueous content (Figure 7). This phenomenon is accounted for by a transient perturbation that stops after a while. Graded release operated in a system requiring high peptide membrane loads for leakage activation (POPC), but also in a system less demanding in terms of the number of peptides per vesicle required for the induction of the process (POPC:SPM) (Figures 6-8). N-preTM CD spectrum in DPC was consistent with peptides adopting a helical

conformation, possibly in monomeric form, as was also evidenced by SDS-PAGE gel analysis (Figures 4 and 5). These observations argue that permeation elicited by N-preTM might not depend on the establishment of strong peptide-peptide interactions at the membrane surface.

In contrast, PreTM-C induced leakage following an all-or-none mechanism (Figure 7). Again, this mechanism was valid for leakage processes requiring high (≈1:100) and low (≈1:1000) peptide-to-lipid membrane ratios for completion (Figures 6-8). In addition, PreTM-C migrated as dimers in SDS-PAGE (Figure 4). The fact that the 4E10 epitope is present in both, the monomeric N-preTM and the dimeric PreTM-C, suggests that the common ^{671}NWFN/DITNWLW^{683} sequence has little effect on this phenomenon. Thus, we infer that formation of SDS-resistant PreTM-C dimers overall depends on the ^{684}LFIMIVGGLV^{693} TMD stretch. To our knowledge the oligomerization of similar HIV-1 TMD peptides has not been reported before. The physiologically relevant oligomeric state of gp41 is assumed to be trimeric. Accordingly, we speculate that the PreTM-C dimers observed in our study are related to the mechanism of pore-formation by this peptide (see below).

The PreTM-C peptide shared several features with the cytolytic honey-bee venom peptide melittin. Both were dimeric in SDS micelles (Figure 4), and induced solute release from vesicles following an all-or-none mechanism that was stimulated by SPM (Figure 7 and reference (*37*)). In addition, both assemble permeating structures of comparable size (*37, 45, 46*). However, previous mathematical modeling of the leakage process yielded K_s values in the range of 0.5 for melittin interacting with POPC:SPM (1:1) vesicles (*37*), indicating a higher degree of irreversible aggregation-insertion for this peptide as compared to PreTM-C (Table 2). The higher efficiency of melittin might reflect an adaptation of its sequence in order to fulfill the pore-forming function in the

context of free peptides interacting with natural zwitterionic membranes. By comparison, the membrane-disrupting activity of PreTM-C is probably optimal when functioning as a constituent of the HIV-1 fusion machinery (*10, 38, 50*).

In this regard, the findings described in this work further support an active role for gp41 MPER in the generation of the stresses required for fusing membranes than just acting as a force-transmitting anchor (*20*). The MPER sequence represented by N-preTM has been postulated to exist in two alternative states in native Env protein: either accessible to solvent within the gp41 stem (*51*), or inserted into the external membrane monolayer of the virion (*52, 53*). Our results suggest that the shallow insertion of this region into the interface might induce transient membrane discontinuities. This rupture effect might increase the propensity of the contacting viral and cell bilayers to hemifuse (*7*).

On the other hand, PreTM-C including an invariant TMD region is predicted to act by inserting its carboxy-terminal end deeper into the hydrocarbon core of the bilayer (Table 1). By analogy with the Trp-rich pore-forming peptides (*10, 21*), PreTM-C might reduce the monolayer bending energy and promote positive spontaneous curvature therein. Induction of this type of spontaneous curvature at the external monolayer might be related to the fusion-pore expansion at the late stages of the fusion process (*7*). Nonetheless, we cannot dismiss the possibility that formation of pores in the fusing viral membrane by MPER-TMD might actually constitute an integral step of the gp41-induced fusion mechanism, as previously suggested by others (*38, 50*). It has been argued that holes created within hemifused membranes may elicit fusion pore completion (*54, 55*). The observation that expression and activation of gp41 results in cell lysis would also support an intrinsic pore-forming activity for this protein (discussed in (*55*)).

Finally, the observations reported by Dimitrov et al. (*56*) indicating that changes in exposure of MPER epitopes occur independently of 6-helix bundle formation is also in accordance with distinct MPER function and dynamics during the course of gp41-induced fusion reaction. These authors found that the loss of epitope exposure and the inhibition by the C34 peptide of 6-helix bundle completion occurred more or less concomitantly. However, addition of C34 did not counteract the loss of antibody binding. They hypothesized that an inward curvature of the viral membrane rather than MPER-lipid interactions would be responsible for the loss of reactivity. The results in the present work put forward the possibility that epitope exposure of membrane-bound MPER sequence might actually be dependent on distinct membrane interactions ensuing along the fusion pathway (Figure 3). Recapitulating these interactions in model systems will require the selection of increasingly complex specimens that reflect bona fide functions of the complete glycoprotein. Meanwhile, efforts leading to such a successful reconstitution approach might help elucidating several aspects of the gp41-induced membrane fusion mechanism, and suggest at the same time new strategies for effective immunogen design.

References:

(1) Doms, R. W., and Moore, J. P. (2000) HIV-1 membrane fusion: targets of opportunity. *J Cell Biol 151*, F9-14.

(2) Eckert, D. M., and Kim, P. S. (2001) Mechanisms of viral membrane fusion and its inhibition. *Annu Rev Biochem 70*, 777-810.

(3) Gallo, S. A., Finnegan, C. M., Viard, M., Raviv, Y., Dimitrov, A., Rawat, S. S., Puri, A., Durell, S., and Blumenthal, R. (2003) The HIV Env-mediated fusion reaction. *Biochim Biophys Acta 1614*, 36-50.

(4) Gallaher, W. R. (1987) Detection of a fusion peptide sequence in the transmembrane protein of human immunodeficiency virus. *Cell 50*, 327-328.

(5) Epand, R. M. (2003) Fusion peptides and the mechanism of viral fusion. *Biochim Biophys Acta 1614*, 116-121.

(6) Nieva, J. L., and Agirre, A. (2003) Are fusion peptides a good model to study viral cell fusion? *Biochim Biophys Acta 1614*, 104-115.

(7) Chernomordik, L. V., and Kozlov, M. M. (2008) Mechanics of membrane fusion. *Nat Struct Mol Biol 15*, 675-683.

(8) Salzwedel, K., West, J. T., and Hunter, E. (1999) A conserved tryptophan-rich motif in the membrane-proximal region of the human immunodeficiency virus type 1 gp41 ectodomain is important for Env-mediated fusion and virus infectivity. *J Virol 73*, 2469-2480.

(9) Munoz-Barroso, I., Salzwedel, K., Hunter, E., and Blumenthal, R. (1999) Role of the membrane-proximal domain in the initial stages of human immunodeficiency virus type 1 envelope glycoprotein-mediated membrane fusion. *J Virol 73*, 6089-6092.

(10) Vishwanathan, S. A., and Hunter, E. (2008) Importance of the membrane-perturbing properties of the membrane-proximal external region of human immunodeficiency virus type 1 gp41 to viral fusion. *J Virol 82*, 5118-5126.

(11) Vishwanathan, S. A., Thomas, A., Brasseur, R., Epand, R. F., Hunter, E., and Epand, R. M. (2008) Hydrophobic substitutions in the first residue of the CRAC segment of the gp41 protein of HIV. *Biochemistry 47*, 124-130.

(12) Suarez, T., Gallaher, W. R., Agirre, A., Goni, F. M., and Nieva, J. L. (2000) Membrane interface-interacting sequences within the ectodomain of the human immunodeficiency virus type 1 envelope glycoprotein: putative role during viral fusion. *J Virol 74*, 8038-8047.

(13) Saez-Cirion, A., Arrondo, J. L., Gomara, M. J., Lorizate, M., Iloro, I., Melikyan, G., and Nieva, J. L. (2003) Structural and functional roles of HIV-1 gp41 pretransmembrane sequence segmentation. *Biophys J 85*, 3769-3780.

(14) Schibli, D. J., Montelaro, R. C., and Vogel, H. J. (2001) The membrane-proximal tryptophan-rich region of the HIV glycoprotein, gp41, forms a well-defined helix in dodecylphosphocholine micelles. *Biochemistry 40*, 9570-9578.

(15) Sun, Z. Y., Oh, K. J., Kim, M., Yu, J., Brusic, V., Song, L., Qiao, Z., Wang, J. H., Wagner, G., and Reinherz, E. L. (2008) HIV-1 broadly neutralizing antibody extracts its epitope from a kinked gp41 ectodomain region on the viral membrane. *Immunity 28*, 52-63.

(16) Roux, K. H., and Taylor, K. A. (2007) AIDS virus envelope spike structure. *Curr Opin Struct Biol 17*, 244-252.

(17) Shnaper, S., Sackett, K., Gallo, S. A., Blumenthal, R., and Shai, Y. (2004) The C- and the N-terminal regions of glycoprotein 41 ectodomain fuse membranes enriched and not enriched with cholesterol, respectively. *J Biol Chem 279*, 18526-18534.

(18) Saez-Cirion, A., Nir, S., Lorizate, M., Agirre, A., Cruz, A., Perez-Gil, J., and Nieva, J. L. (2002) Sphingomyelin and cholesterol promote HIV-1 gp41 pretransmembrane sequence surface aggregation and membrane restructuring. *J Biol Chem 277*, 21776-21785.

(19) Brugger, B., Glass, B., Haberkant, P., Leibrecht, I., Wieland, F. T., and Krausslich, H. G. (2006) The HIV lipidome: a raft with an unusual composition. *Proc Natl Acad Sci U S A 103*, 2641-2646.

(20) Lorizate, M., Huarte, N., Saez-Cirion, A., and Nieva, J. L. (2008) Interfacial pre-transmembrane domains in viral proteins promoting membrane fusion and fission. *Biochim Biophys Acta 1778*, 1624-1639.

(21) Chan, D. I., Prenner, E. J., and Vogel, H. J. (2006) Tryptophan- and arginine-rich antimicrobial peptides: structures and mechanisms of action. *Biochim Biophys Acta 1758*, 1184-1202.

(22) Huarte, N., Lorizate, M., Maeso, R., Kunert, R., Arranz, R., Valpuesta, J. M., and Nieva, J. L. (2008) The broadly neutralizing anti-human immunodeficiency virus type 1 4E10 monoclonal antibody is better adapted to membrane-bound epitope recognition and blocking than 2F5. *J Virol 82*, 8986-8996.

(23) Lorizate, M., Cruz, A., Huarte, N., Kunert, R., Perez-Gil, J., and Nieva, J. L. (2006) Recognition and blocking of HIV-1 gp41 pre-transmembrane sequence by monoclonal 4E10 antibody in a Raft-like membrane environment. *J Biol Chem 281*, 39598-39606.

(24) Montero, M., van Houten, N. E., Wang, X., and Scott, J. K. (2008) The membrane-proximal external region of the human immunodeficiency virus type 1 envelope: dominant site of antibody neutralization and target for vaccine design. *Microbiol Mol Biol Rev 72*, 54-84.

(25) Sanchez-Martinez, S., Lorizate, M., Katinger, H., Kunert, R., and Nieva, J. L. (2006) Membrane association and epitope recognition by HIV-1 neutralizing anti-gp41 2F5 and 4E10 antibodies. *AIDS Res Hum Retroviruses 22*, 998-1006.

(26) White, S. H., Wimley, W. C., Ladokhin, A. S., and Hristova, K. (1998) Protein folding in membranes: determining energetics of peptide-bilayer interactions. *Methods Enzymol 295*, 62-87.

(27) Bolen, E. J., and Holloway, P. W. (1990) Quenching of tryptophan fluorescence by brominated phospholipid. *Biochemistry 29*, 9638-9643.

(28) De Kroon, A. I., Soekarjo, M. W., De Gier, J., and De Kruijff, B. (1990) The role of charge and hydrophobicity in peptide-lipid interaction: a comparative study based on tryptophan fluorescence measurements combined with the use of aqueous and hydrophobic quenchers. *Biochemistry 29*, 8229-8240.

(29) Ellens, H., Bentz, J., and Szoka, F. C. (1985) H+- and Ca2+-induced fusion and destabilization of liposomes. *Biochemistry 24*, 3099-3106.

(30) Basanez, G., Zhang, J., Chau, B. N., Maksaev, G. I., Frolov, V. A., Brandt, T. A., Burch, J., Hardwick, J. M., and Zimmerberg, J. (2001) Pro-apoptotic

cleavage products of Bcl-xL form cytochrome c-conducting pores in pure lipid membranes. *J Biol Chem 276*, 31083-31091.

(31) Wimley, W. C., Selsted, M. E., and White, S. H. (1994) Interactions between human defensins and lipid bilayers: evidence for formation of multimeric pores. *Protein Sci 3*, 1362-1373.

(32) Ladokhin, A. S., Wimley, W. C., and White, S. H. (1995) Leakage of membrane vesicle contents: determination of mechanism using fluorescence requenching. *Biophys J 69*, 1964-1971.

(33) Ladokhin, A. S., Wimley, W. C., Hristova, K., and White, S. H. (1997) Mechanism of leakage of contents of membrane vesicles determined by fluorescence requenching. *Methods Enzymol 278*, 474-486.

(34) Rausch, J. M., Marks, J. R., Rathinakumar, R., and Wimley, W. C. (2007) Beta-sheet pore-forming peptides selected from a rational combinatorial library: mechanism of pore formation in lipid vesicles and activity in biological membranes. *Biochemistry 46*, 12124-12139.

(35) Nicol, F., Nir, S., and Szoka, F. C., Jr. (1996) Effect of cholesterol and charge on pore formation in bilayer vesicles by a pH-sensitive peptide. *Biophys J 71*, 3288-3301.

(36) Nir, S., and Nieva, J. L. (2000) Interactions of peptides with liposomes: pore formation and fusion. *Prog Lipid Res 39*, 181-206.

(37) Gomara, M. J., Nir, S., and Nieva, J. L. (2003) Effects of sphingomyelin on melittin pore formation. *Biochim Biophys Acta 1612*, 83-89.

(38) Shang, L., Yue, L., and Hunter, E. (2008) Role of the membrane-spanning domain of human immunodeficiency virus type 1 envelope glycoprotein in cell-cell fusion and virus infection. *J Virol 82*, 5417-5428.

(39) White, S. H. (2003) Translocons, thermodynamics, and the folding of membrane proteins. *FEBS Lett 555*, 116-121.

(40) McIntosh, T. J., and Holloway, P. W. (1987) Determination of the depth of bromine atoms in bilayers formed from bromolipid probes. *Biochemistry 26*, 1783-1788.

(41) Zwick, M. B., Jensen, R., Church, S., Wang, M., Stiegler, G., Kunert, R., Katinger, H., and Burton, D. R. (2005) Anti-human immunodeficiency virus type 1 (HIV-1) antibodies 2F5 and 4E10 require surprisingly few crucial residues in the membrane-proximal external region of glycoprotein gp41 to neutralize HIV-1. *J Virol 79*, 1252-1261.

(42) Keating, A. E., Malashkevich, V. N., Tidor, B., and Kim, P. S. (2001) Side-chain repacking calculations for predicting structures and stabilities of heterodimeric coiled coils. *Proc Natl Acad Sci U S A 98*, 14825-14830.

(43) Litowski, J. R., and Hodges, R. S. (2002) Designing heterodimeric two-stranded alpha-helical coiled-coils. Effects of hydrophobicity and alpha-helical propensity on protein folding, stability, and specificity. *J Biol Chem 277*, 37272-37279.

(44) Zhu, P., Chertova, E., Bess, J., Jr., Lifson, J. D., Arthur, L. O., Liu, J., Taylor, K. A., and Roux, K. H. (2003) Electron tomography analysis of envelope glycoprotein trimers on HIV and simian immunodeficiency virus virions. *Proc Natl Acad Sci U S A 100*, 15812-15817.

(45) Ladokhin, A. S., Selsted, M. E., and White, S. H. (1997) Sizing membrane pores in lipid vesicles by leakage of co-encapsulated markers: pore formation by melittin. *Biophys J 72*, 1762-1766.

(46) Ladokhin, A. S., and White, S. H. (2001) 'Detergent-like' permeabilization of anionic lipid vesicles by melittin. *Biochim Biophys Acta 1514*, 253-260.

(47) Benachir, T., and Lafleur, M. (1995) Study of vesicle leakage induced by melittin. *Biochim Biophys Acta 1235*, 452-460.

(48) Nicol, F., Nir, S., and Szoka, F. C., Jr. (2000) Effect of phospholipid composition on an amphipathic peptide-mediated pore formation in bilayer vesicles. *Biophys J 78*, 818-829.

(49) Rapaport, D., Peled, R., Nir, S., and Shai, Y. (1996) Reversible surface aggregation in pore formation by pardaxin. *Biophys J 70*, 2502-2512.

(50) Arroyo, J., Boceta, M., Gonzalez, M. E., Michel, M., and Carrasco, L. (1995) Membrane permeabilization by different regions of the human immunodeficiency virus type 1 transmembrane glycoprotein gp41. *J Virol 69*, 4095-4102.

(51) Zanetti, G., Briggs, J. A., Grunewald, K., Sattentau, Q. J., and Fuller, S. D. (2006) Cryo-electron tomographic structure of an immunodeficiency virus envelope complex in situ. *PLoS Pathog 2*, e83.

(52) Zhu, P., Liu, J., Bess, J., Jr., Chertova, E., Lifson, J. D., Grise, H., Ofek, G. A., Taylor, K. A., and Roux, K. H. (2006) Distribution and three-dimensional structure of AIDS virus envelope spikes. *Nature 441*, 847-852.

(53) Zhu, P., Winkler, H., Chertova, E., Taylor, K. A., and Roux, K. H. (2008) Cryoelectron tomography of HIV-1 envelope spikes: further evidence for tripod-like legs. *PLoS Pathog 4*, e1000203.

(54) Muller, M., Katsov, K., and Schick, M. (2003) A new mechanism of model membrane fusion determined from Monte Carlo simulation. *Biophys J 85*, 1611-1623.

(55) Engel, A., and Walter, P. (2008) Membrane lysis during biological membrane fusion: collateral damage by misregulated fusion machines. *J Cell Biol 183*, 181-186.

(56) Dimitrov, A. S., Jacobs, A., Finnegan, C. M., Stiegler, G., Katinger, H., and Blumenthal, R. (2007) Exposure of the membrane-proximal external region of HIV-1 gp41 in the course of HIV-1 envelope glycoprotein-mediated fusion. *Biochemistry 46*, 1398-1401.

(57) Wimley, W. C., and White, S. H. (1996) Experimentally determined hydrophobicity scale for proteins at membrane interfaces. *Nat Struct Biol 3*, 842-848.

(58) Kyte, J., and Doolittle, R. F. (1982) A simple method for displaying the hydropathic character of a protein. *J Mol Biol 157*, 105-132.

Table 1: Energetics of the interaction of MPER sequences with phospholipid bilayers

Sequence[1]	HIV-1 Env numbering[1]	ΔG_{wi}[2]	ΔG_{wo}[2]	ΔG_{io}[2]
NEQELLELDKWASLWNWFNITNWLWYIK	656-683	-2.8	+4.1	+6.9
NWFNITNWLWYIKLFIMIVGGLV	671-693	-9.3	-12.3	-3.0

1: Sequences and numbering based on the HXBc2 reference isolate.

2: The free energies of transferring (Kcal mol^{-1}) from water into interface (wi), water into octanol (wo) and interface into octanol (io) as described in reference (*39*).

Table 2: Summary of calculations to obtain the best fits of final extents of ANTS/DPX leakage induced by PreTM-C.

Lipid Composition	M	K_S	R^2
POPC	6	0.0075	0.90
	8	0.0150	0.90
POPC:SPM	6	0.0220	0.90
	8	0.0430	0.90

Figure legends

Figure 1: Hydrophobicity distribution within the membrane proximal and transmembrane regions of the HIV-1 gp41 integral subunit (top) and derived peptides (bottom). The average hydropathy plots were produced as follows: Black solid: a window of 5 amino acids was used with the WW hydrophobicity scale at membrane interfaces (*57*); Red dotted: the WW moment (window of 11 amino acids) was calculated for a fixed $\delta = 100^{o}$ (helical periodicity) and hydrophobicity-at-interface scale (*13*); Blue solid: a window of 5 amino acids was used with the KD hydropathy index (*58*). Sequence and numbering according to the prototypic HXBc2 isolate.

Figure 2: Association with membranes of N-preTM and PreTM-C (right and left panels, respectively). A) Partition into POPC bilayers. Fluorescence emission spectra (excitation wavelength: 280 nm) of peptides, in solution (dotted) or when incubated in the presence of POPC LUV (black spectra). Peptide and lipid concentrations were 0.5 and 100 μM, respectively. B) Partitioning curves estimated from the fractional change in Trp fluorescence with increasing POPC concentrations. Means ± S.D. of 3 independent experiments are represented. The solid line corresponds to the best fit of the experimental values to Eq. [1] and the calculated $K_{x(app)}$ are displayed in the panels. Conditions otherwise as in the previous panel. C) Stern-Volmer plots of quenching by Br_6-PSPC (filled circles and solid lines) or Br_{11}-PSPC (empty circles and dotted lines). Means ± S.D. of 3 independent experiments are represented. The panels show the K_{sv} values in μM^{-1} as inferred from the linear regressions following Eq. [2]. D) Final extents

of ANTS leakage (percentage after 30 minutes) from POPC LUV as a function of peptide-to-lipid mole ratio (R_i). Lipid concentration (100 μM) was fixed.

Figure 3: Differential blocking of N-preTM or PreTM-C-induced permeabilization displayed by the 4E10 MAb in POPC vesicles. A) The binding of 4E10 MAb to 1.4 μM N-preTM (left) or PreTM-C (right) immobilized on ELISA plates. The empty symbols correspond to the N-preTM$_{mut}$ and PreTM-C$_{mut}$ mutant variants. B) Inhibition of ongoing ANTS leakage. LUV suspensions (100 μM lipid) were treated with 1 μM (N-preTM and N-preTM$_{mut}$) or 0.4 μM (PreTM-C and PreTM-C$_{mut}$) peptide and subsequently they were supplemented with 20 μg/ml (N-preTM and N-preTM$_{mut}$) or 50 μg/ml (PreTM-C and PreTM-C$_{mut}$) of the 4E10 MAb (addition times indicated by "a" and "b", respectively). Dotted traces correspond to the controls in the absence of antibody. C) Inhibition of ANTS leakage by pre-incubation of the peptides with the MAb 4E10 in solution ("a,b"). At the time indicated by "LUV" the ANTS/DPX-containing vesicles were added to the mixture. Conditions otherwise as in the previous panel.

Figure 4: CD spectra of N-preTM (left) and PreTM-C (right) peptides in DPC micelles (20 mM). The peptide concentration was 30 μM in both samples.

Figure 5: SDS-PAGE analysis of MPER-derived peptides and melittin. Peptides were loaded in a tricine gel and blue-stained with Coomasie. M: M_r markers. Lane 1: 1.5 μg of PreTM-C; Lane 2: 25 μg of PreTM-C; Lane 3: 25 μg of N-preTM; Lane 4: 25 μg of melittin.

Figure 6: Effect of SPM on N-preTM (left) and PreTM-C (right) partitioning and induced LUV permeabilization. A) Partitioning curves estimated from the fractional change in Trp fluorescence with increasing POPC:SPM (1:1) concentrations. Means ± S.D. of 3 independent experiments are represented. The solid line corresponds to the best fit of the experimental values to Eq. [1] and the calculated $K_{x(app)}$ are displayed in the panels. The peptide concentration was 0.5 μM. B) Kinetics and final extents of ANTS leakage (top and bottom panels, respectively). Top panels: peptide was added to POPC:SPM (1:1 mole ratio) or POPC vesicle suspensions at a peptide-to-lipid ratio of 1:500 (solid and slashed lines, respectively). Time of addition, t = 50 s. The lipid concentration was 100 μM. Bottom panels: final extents of leakage (percentage of ANTS released after 30 minutes) in POPC:SM (1:1) as a function of peptide-to-lipid mole ratio (R_i) in the membrane. The lipid concentration was 100 μM.

Figure 7: Fluorescence requenching assays to establish the mechanism of membrane permeabilization in POPC and POPC:SPM vesicles (left and right panel, respectively). Internal quenching (Q_{in}) was measured as a function of the ANTS released (f_{out}) after incubation with N-preTM, PreTM-C or melttin (filled circles, empty circles and filled squares, respectively). Means ± S.D. of 3 independent experiments are represented. The lines correspond to the best fit of the experimental values using the basic equation of the requenching technique as described by Ladokhin et al. (*32, 33*). The solid lines indicate that N-preTM induced a graded release of ANTS/DPX from POPC and POPC:SPM vesicles, which is preferential for DPX (α values of 2.2 and 1.5, respectively). The dotted lines correspond to graded release simulated for nonpreferential release (α=1).

The horizontal dashed lines denote the expected behavior for all-or-none processes and fit the experimental values obtained for PreTM-C and melittin.

Figure 8: Final extents of PreTM-C-induced leakage (percentage after 30 min) in POPC and POPC:SPM (1:1 mol:mol) vesicles as a function of the lipid-to-peptide mole ratio (left and right panels, respectively). The lipid concentration was constant (100 μM). The dotted curves correspond to the predicted values calculated for a pore model in which the minimal number of monomers required for pore formation was M=8.

Figure 9: Leakage of solutes of different sizes encapsulated into POPC:SPM (1:1) vesicles. The capacities of PreTM-C (top) and N-preTM (bottom) to induce release of ANTS (MW: 425, circles), FD-4 (MW: 4,000, squares), and FD-20 (MW: 20,000, diamonds) and FD-40 (MW: 40,000, triangles) are compared. Final extent values were obtained upon incubation of peptides and vesicles for 30 minutes at different peptide-to lipid molar ratios (R_i). The lipid concentration was 100 μM.

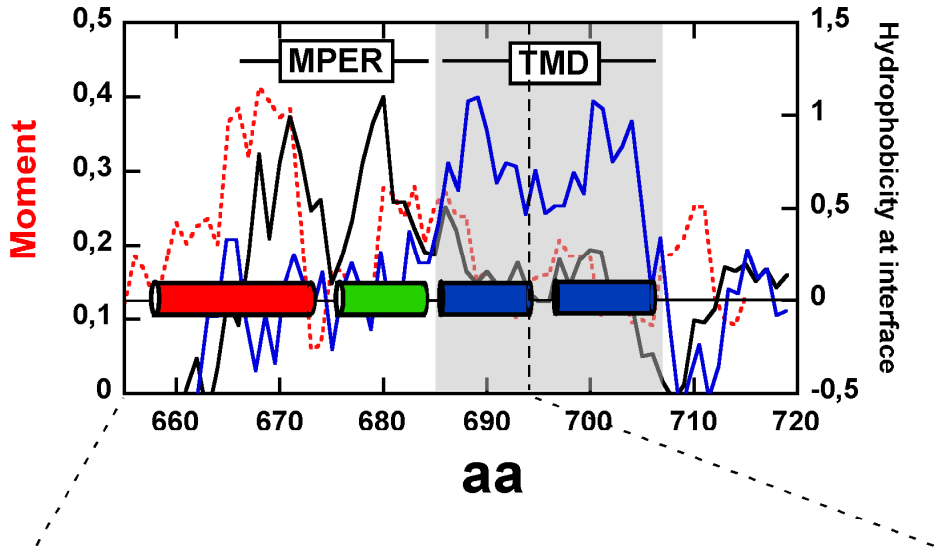

656NEQELLELDKWASLW670-671NWFXITNWLWYIK683-684LFIMIVGGLV693

4E10

N-preTM: 656NEQELLELDKWASLW670-671NWFNITNWLWYIK683

PreTM-C: *KKK*671NWFDITNWLWYIK683-684LFIMIVGGLV693*KK*

Fig.1

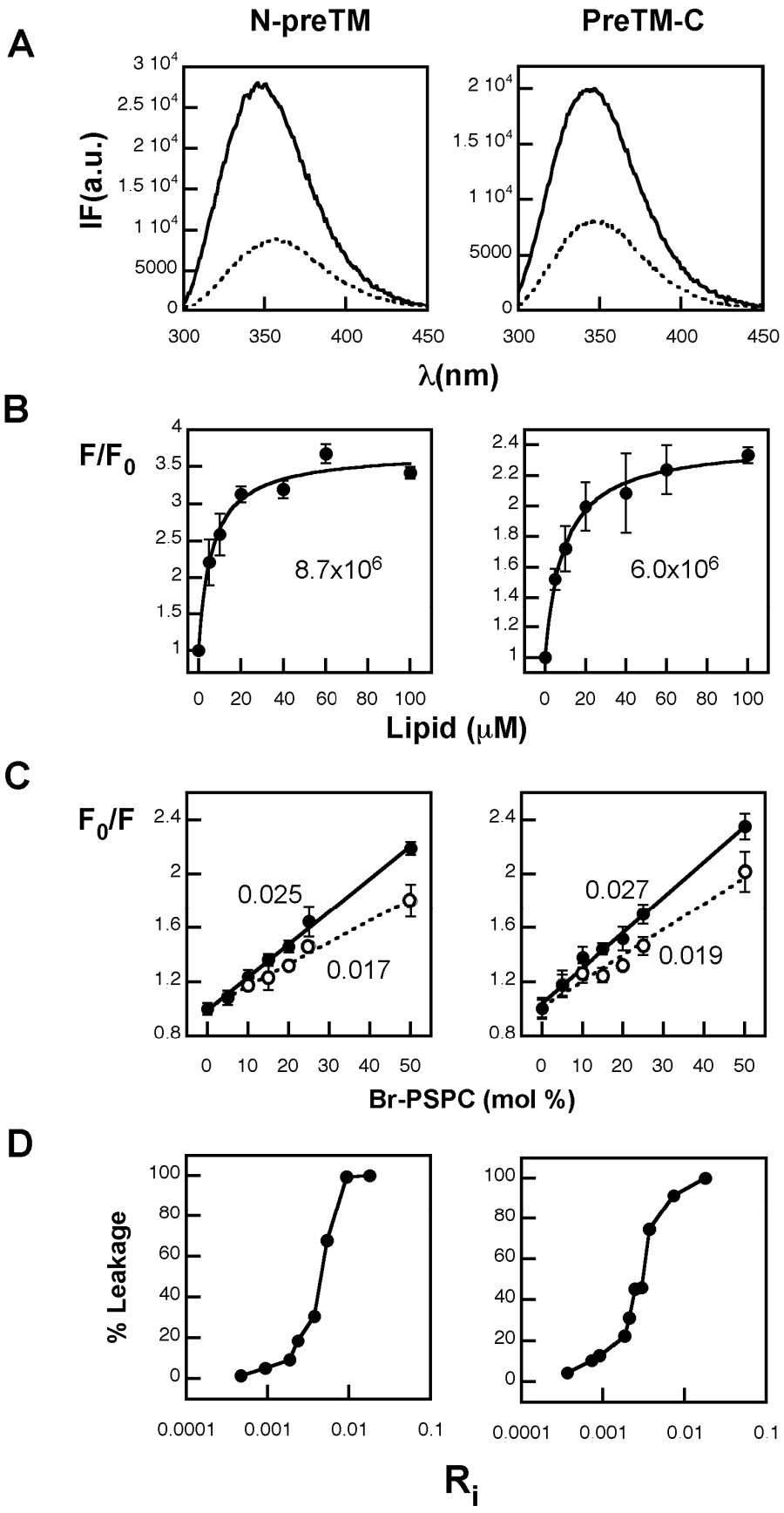
A
N-preTM
PreTM-C
IF(a.u.)
λ(nm)
B
F/F0
8.7x10^6
6.0x10^6
Lipid (μM)
C
F0/F
0.025
0.017
0.027
0.019
Br-PSPC (mol %)
D
% Leakage
Ri

Fig. 2

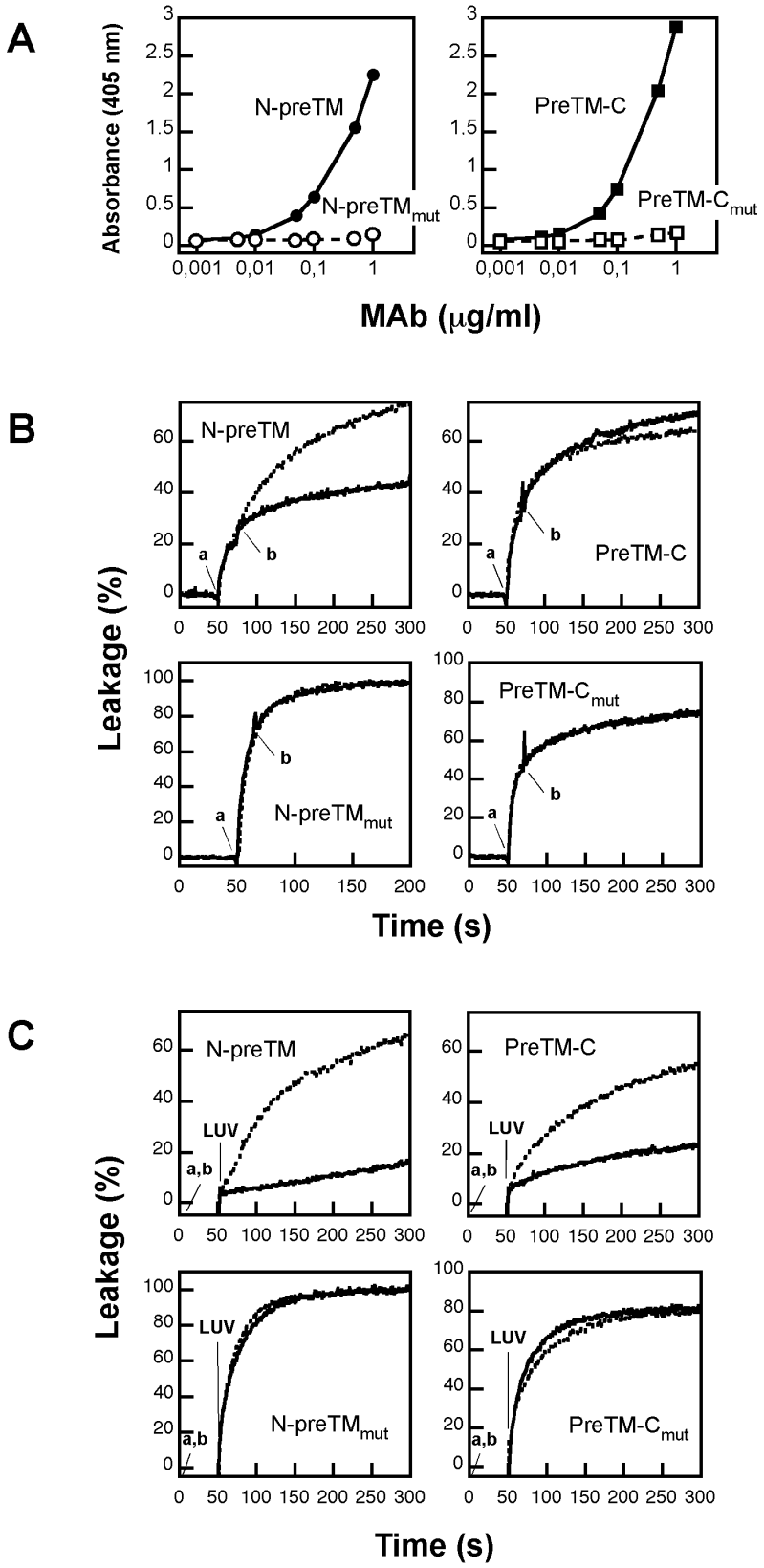
A
Absorbance (405 nm)
N-preTM
N-preTM$_{mut}$
PreTM-C
PreTM-C$_{mut}$
MAb (μg/ml)
B
Leakage (%)
N-preTM
PreTM-C
N-preTM$_{mut}$
PreTM-C$_{mut}$
a
b
Time (s)
C
Leakage (%)
LUV
a,b
N-preTM
PreTM-C
N-preTM$_{mut}$
PreTM-C$_{mut}$
Time (s)

Fig. 3

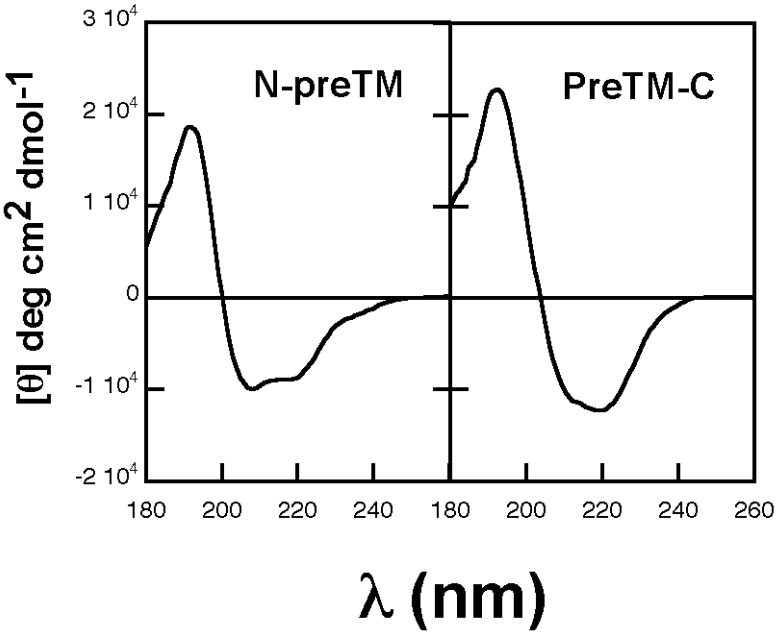
N-preTM
PreTM-C
[θ] deg cm2 dmol-1
3 10^4
2 10^4
1 10^4
0
-1 10^4
-2 10^4
180
200
220
240
180
200
220
240
260
λ (nm)

Fig. 4

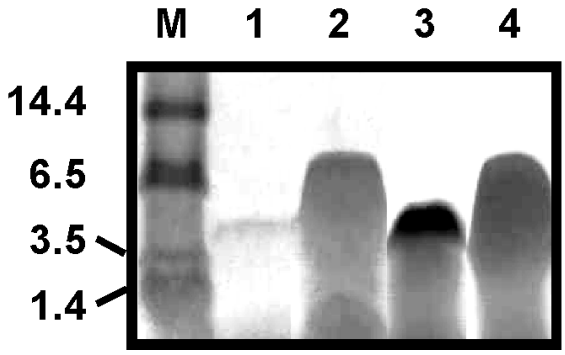

Fig. 5

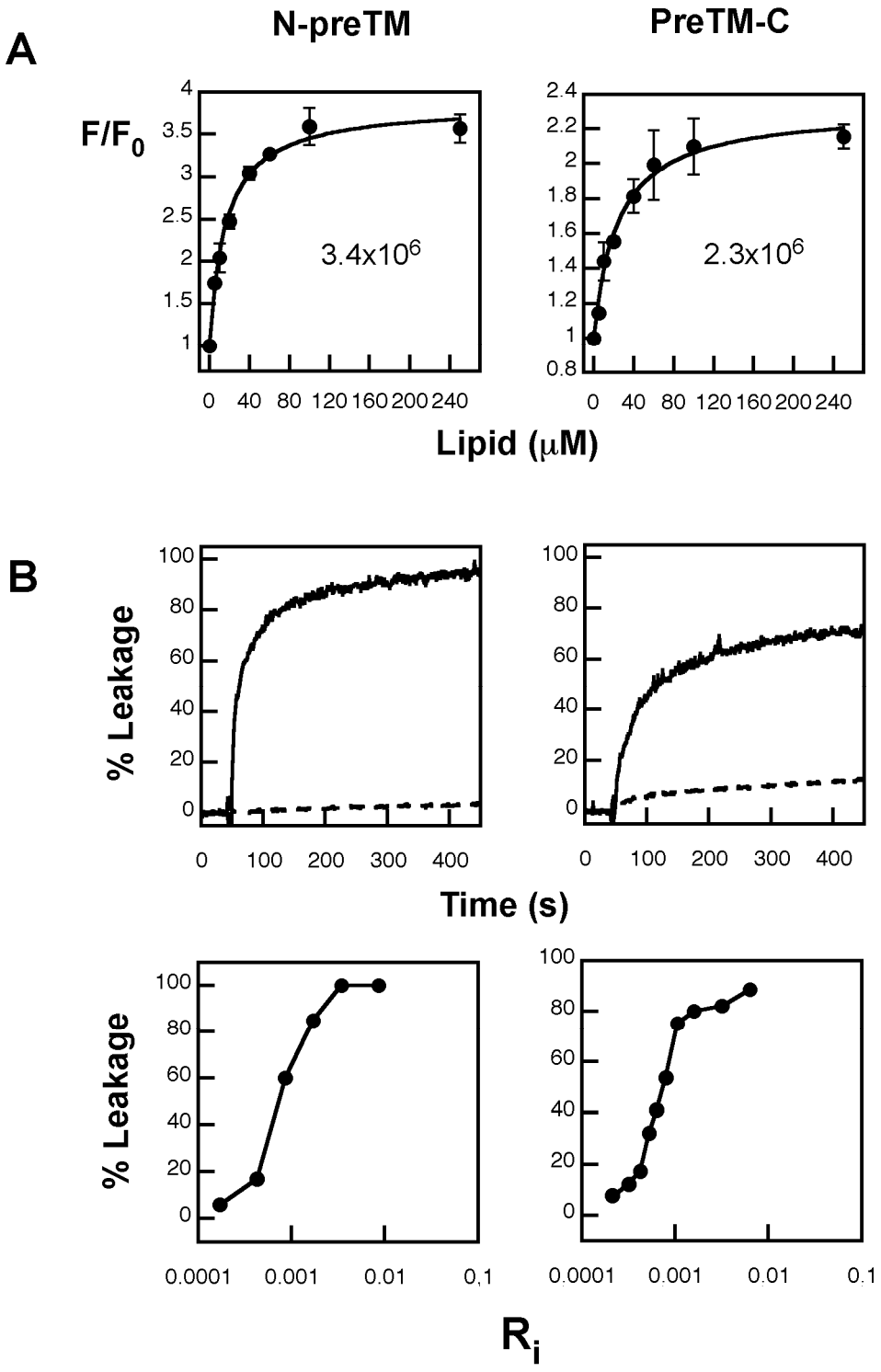
A
N-preTM
PreTM-C
F/F0
3.4x10^6
2.3x10^6
Lipid (μM)
B
% Leakage
Time (s)
% Leakage
Ri

Fig. 6

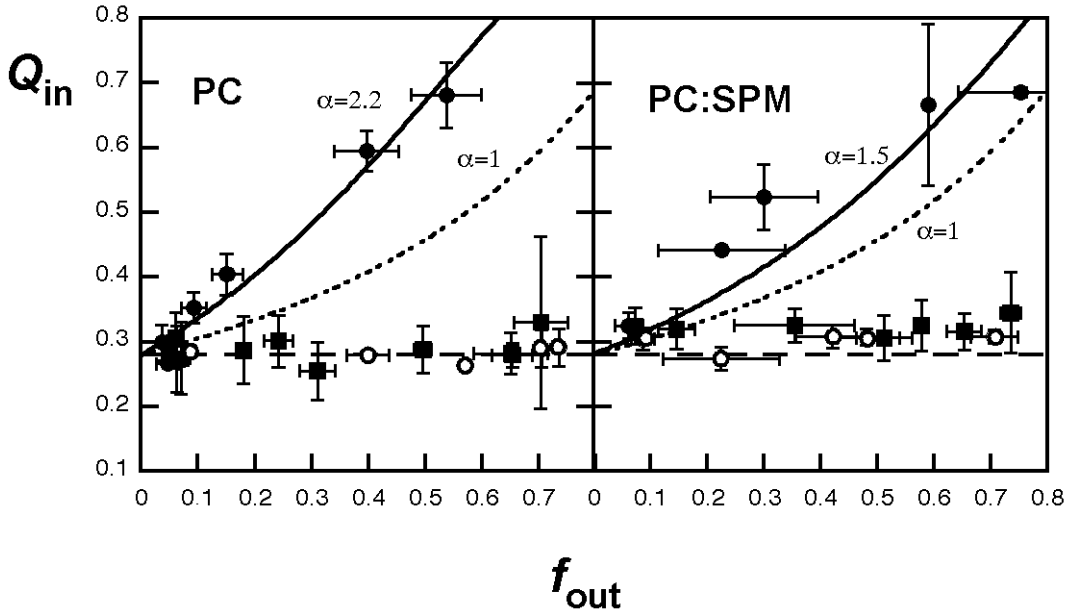

Fig. 7

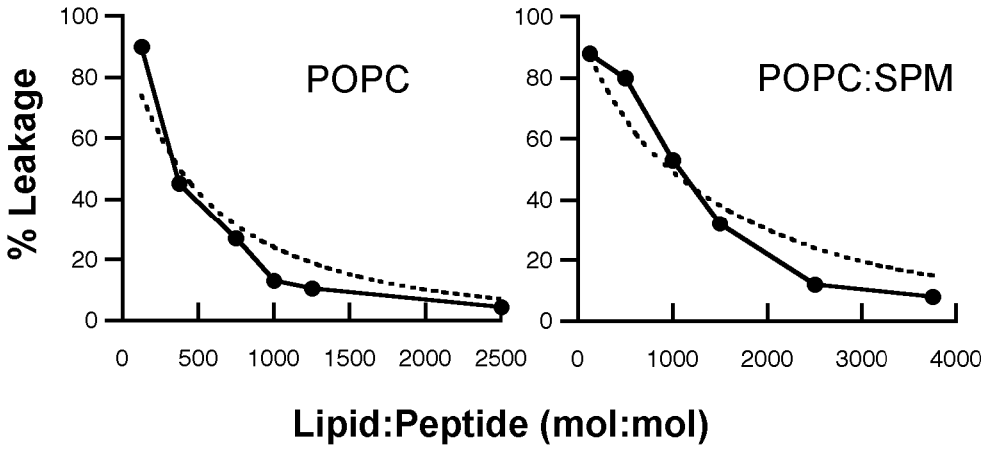
% Leakage
100
80
60
40
20
0
POPC
0
500
1000
1500
2000
2500
POPC:SPM
0
1000
2000
3000
4000
Lipid:Peptide (mol:mol)

Fig. 8

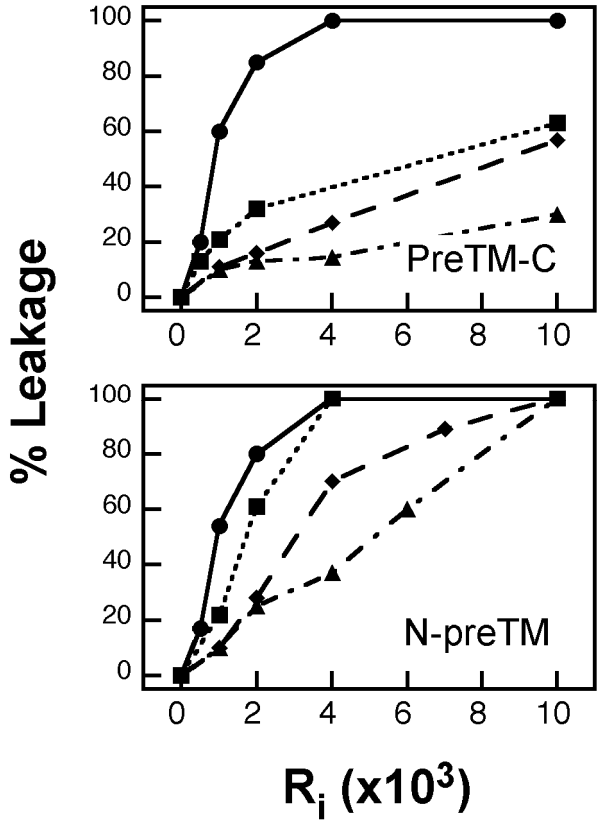

Fig. 9

For table of contents use only

DISTINCT MECHANISMS OF LIPID BILAYER PERTURBATION BY PEPTIDES DERIVED FROM THE MEMBRANE-PROXIMAL EXTERNAL REGION OF HIV-1 gp41

Beatriz Apellániz, Shlomo Nir, and José L. Nieva